ACS APPLIED MATERIALS & INTERFACES

Research Article

Cite This: ACS Appl. Mater. Interfaces XXXX, XXX, XXX−XXX

www.acsami.org

Tunable Resonance Coupling in Single Si Nanoparticle−Monolayer WS_2 Structures

Sergey Lepeshov,[†] Mingsong Wang,[‡] Alex Krasnok,[*,§] Oleg Kotov,[∥] Tianyi Zhang,[⊥] He Liu,[#] Taizhi Jiang,[♦] Brian Korgel,[♦] Mauricio Terrones,[⊥,#,¶,▽,○] Yuebing Zheng,[*,‡] and Andrea Alú[*,§,††,△,⬢]

[†]ITMO University, St. Petersburg 197101, Russia

[‡]Department of Mechanical Engineering, Texas Materials Institute, [§]Department of Electrical and Computer Engineering, and [♦]McKetta Department of Chemical Engineering and Texas Materials Institute, The University of Texas at Austin, Austin, Texas 78712, United States

[∥]Institute of MicroelectronicsTechnology and High Purity Materials, Russian Academy of Sciences, 142432 Chernogolovka, Russia

[⊥]Department of Materials Science and Engineering and Center for 2-Dimensional and Layered Materials, [#]Department of Chemistry and Center for 2-Dimensional and Layered Materials, and [¶]Department of Physics, The Pennsylvania State University, University Park, Pennsylvania 16802, United States

[▽]Department of Materials Science and Engineering & Chemical Engineering, Carlos III University of Madrid, Avenida Universidad 30, Leganés, Madrid 28911, Spain

[○]IMDEA Materials Institute, Eric Kandel 2, Getafe, Madrid 28005, Spain

[††]Photonics Initiative, Advanced Science Research Center, City University of New York, New York, New York 10031, United States

[△]Physics Program, Graduate Center, City University of New York, New York 10016, United States

[⬢]Department of Electrical Engineering, City College of The City University of New York, New York 10031, United States

Supporting Information

ABSTRACT: Two-dimensional semiconducting transition metal dichalcogenides (TMDCs) are extremely attractive materials for optoelectronic applications in the visible and near-infrared range. Coupling these materials to optical nanocavities enables advanced quantum optics and nanophotonic devices. Here, we address the issue of resonance coupling in hybrid exciton−polariton structures based on single Si nanoparticles (NPs) coupled to monolayer (1L)-WS_2. We predict a strong coupling regime with a Rabi splitting energy exceeding 110 meV for a Si NP covered by 1L-WS_2 at the magnetic optical Mie resonance because of the symmetry of the mode. Further, we achieve a large enhancement in the Rabi splitting energy up to 208 meV by changing the surrounding dielectric material from air to water. The prediction is based on the experimental estimation of TMDC dipole moment variation obtained from the measured photoluminescence spectra of 1L-WS_2 in different solvents. An ability of such a system to tune the resonance coupling is realized experimentally for optically resonant spherical Si NPs placed on 1L-WS_2. The Rabi splitting energy obtained for this scenario increases from 49.6 to 86.6 meV after replacing air by water. Our findings pave the way to develop high-efficiency optoelectronic, nanophotonic, and quantum optical devices.

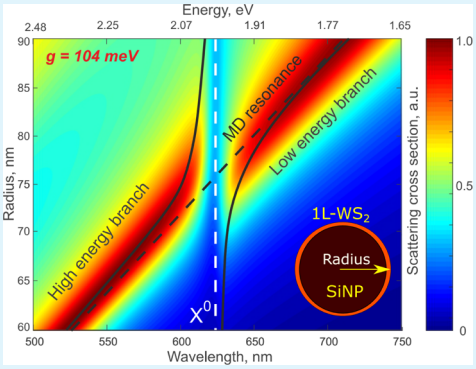

KEYWORDS: *transition metal dichalcogenides, high-index dielectric nanoantennas, magnetic Mie resonance, exciton resonance, strong coupling*

INTRODUCTION

Because of the recent tremendous progress in materials science, many novel materials with unique optoelectronic properties have been recently discovered and explored as they exhibit fascinating applications. One prominent example that has been extensively studied in recent years consists of atomically thin semiconducting transition metal dichalcogenides (TMDCs).[1−6] A monolayer of TMDCs is formed by a hexagonal network of transition metal atoms (Mo and W) hosted between two hexagonal lattices of chalcogenide atoms (S and Se). Electronically, TMDCs behave as two-dimensional (2D) semiconductors with their band gaps lying in the visible and near-infrared

Received: November 10, 2017
Accepted: April 13, 2018
Published: April 13, 2018

DOI: 10.1021/acsami.7b17112
ACS Appl. Mater. Interfaces XXXX, XXX, XXX−XXX

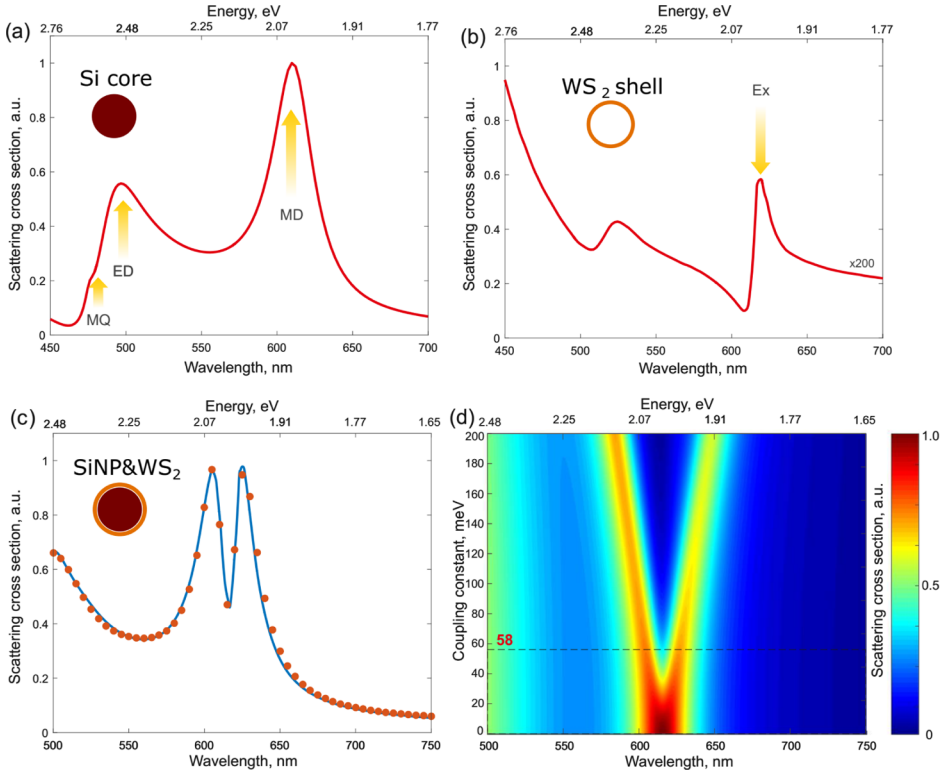

Figure 1. Scattering cross sections of the (a) Si NP of radius R = 75 nm, (b) WS_2 shell with thickness $h \approx 0.7$ nm, and (c) Si-WS_2 core−shell system with the same parameters. Red dots in (c) show the fitting by the coupled mode theory (CMT). (d) Scattering cross section of the Si-WS_2 core−shell system at various coupling constants g. The dotted line at g = 58 meV corresponds to the case shown in (c). The radius of the Si NP is the same as in (a−c) and equals to 75 nm. All results correspond to air environment.

(IR) range. In the atomic monolayer limit, these materials are particularly interesting because their band gap becomes direct, thus enabling enhanced interactions of the dipole transition with light.[7] Because of their monolayer nature, high oscillator strength, and the potential for tuning these materials, they become a unique class of 2D materials in the context of optoelectronic applications, such as photodetection and light harvesting,[8−11] phototransistors and modulation,[12,13] light-emitting diodes,[14−16] and lasers.[17,18]

A variety of new optical effects stem from the interaction between TMDC monolayers and plasmonic (i.e., made of noble metals) nanoscale objects, which have become a goal of extensive studies.[19] Examples include the observation of strong plasmon−exciton coupling,[20−24] pronounced Fano resonance,[25] and plasmon-induced resonance energy transfer[26] among others. These effects benefit from the small mode value of plasmonic resonances and the strong dipole moment of excitons in TMDCs. However, conventional plasmonic materials, such as gold (Au) and silver (Ag), have finite conductivities at optical frequencies, leading to inherent dissipation of electromagnetic energy. This energy loss causes Joule heating of the structure and its local environment.[27,28] For many applications, heat generation in nanostructures is detrimental because the behavior of the excitonic system can be modified dramatically with temperature. Moreover, an excitonic system exhibits quenching when it is placed nearby metallic nanostructures because of the dominant nonradiative decay. We also note that plasmonic nanostructures are not compatible with most semiconductor device processing technologies, thus narrowing the scope of their applicability.

High-index semiconductor (e.g., Si, GaP, and Ge) nanoparticles (NPs) can circumvent these issues, while providing an abundant spectrum of optical functions.[29−35] Here, we address for the first time to the best of our knowledge the resonance coupling in single Si NP−monolayer (1L)-WS_2. The purpose of this paper is twofold. First, we predict to reach the strong coupling regime when Si NPs are covered by 1L-WS_2 at the magnetic optical Mie resonance, with a Rabi splitting energy exceeding 110 meV. The strong coupling regime is achieved owing to the symmetry of the magnetic Mie mode, which allows a strong interaction with atomically thin materials. Moreover, we show that the coupling strength can be largely tuned by changing the surrounding dielectric material and achieve a large enhancement in the Rabi splitting energy up to 208 meV by changing the surrounding dielectric material from air to water. This prediction is based on the experimental estimation of the TMDC dipole moment variation obtained from the measured photoluminescence (PL) spectra of 1L-WS_2 in different solvents (e.g., air and water). We note that a similar core−shell geometry has been recently realized in refs 36 and 37, based on small SiO_2 and Au NPs by chemical vapor deposition (CVD) technology, making a single Si NP-WS_2 core−shell design potentially realizable. Second, the ability of such a system to tune the resonance coupling is demonstrated experimentally in the geometry of optically resonant spherical Si NPs arranged on 1L-WS_2. The values of Rabi splitting energy obtained from fitting the experimental data reveal a significant enhancement (from 49.6 to 86.6 meV), when replacing air by water.

We note that although the Mie magnetic dipole (MD) mode is mainly concentrated inside the Si NP, it has a tail outside the

DOI: 10.1021/acsami.7b17112
ACS Appl. Mater. Interfaces XXXX, XXX, XXX−XXX

NP, enabling efficient coupling with TMDCs, as demonstrated below. Noticeably, in contrast to the electric dipole (ED) mode of spherical plasmonic NPs, the MD mode has a field configuration (tangential component to the particle surface) that couples efficiently to the bright exciton of 1L-WS_2. The ED mode of spherical particles, polarized along the radial direction, does not enable such an effective coupling, and particles with a more complex shape (triangles and rods) are required. In addition, the resonant behavior of a dielectric nanocavity strongly depends on its size, which may be used to tune its resonance to the excitonic response of TMDCs. Moreover, the hot-electron injection from plasmonic nanostructures to TMDCs could lead to the phase change and unwanted doping of TMDCs, which are not desired in many device applications.

RESULTS AND DISCUSSION

We start our analysis by considering a core−shell spherical particle with a silicon (Si) core and a 1L-WS_2 shell. This simple model configuration can be analyzed via analytical methods. First, by using Mie theory,[38] we calculate separately the scattering cross sections of a Si NP and a 1L-WS_2 empty shell with atomic thickness ($h \approx 0.7$ nm), whose dielectric function is determined by reflectance measurements.[39] The dielectric permittivity of c-Si has been taken from ref 40 for ambient temperature $T = 300$ K. For Si NPs, we obtain strong ED and MD resonances (Figure 1a) whose positions depend on the particle radius. The magnetic quadrupole (MQ) resonance can also be observed in the scattering spectrum (for multipole decomposition, see the Supporting Information). By choosing the radius of Si NP $R = 75$ nm, we obtain the MD resonance at $\lambda \approx 615$ nm (~2 eV), at which the electrically neutral exciton (X^0) resonance in WS_2 monolayers takes place.[39] The scattering cross section of the WS_2 shell is 2 orders of magnitude less than that of the Si NP of the same radius (Figure 1b), but it demonstrates a sharp peak (Ex), corresponding to the X^0 exciton in 1L-WS_2.

Then, we use the Mie theory generalized for core−shell spherical particles[41−43] for the calculation of the scattering cross section of the Si NP-WS_2 core−shell system. We use the parameters fitted earlier to achieve the maximum overlap of the MD Mie resonance of Si NPs and the X^0 exciton peak of 1L-WS_2. The interaction of these two resonances gives a strong Fano-like resonance at $\lambda \approx 615$ nm (Figure 1c), for which the coupling constant g can be extracted using CMT. In the harmonic oscillator approximation (for details, see the Supporting Information), the scattering cross section of our system with two coupled oscillators is given by[25,44,45]

$$\sigma_{scat} \propto \left| \frac{\omega^2 \tilde{\omega}_{ex}^{\,2}}{\tilde{\omega}_{md}^{\,2}\tilde{\omega}_{ex}^{\,2} - g^2\omega^2} \right|^2 \quad (1)$$

where $\tilde{\omega}_{ex}^{\,2} = \omega^2 - \omega_{ex}^{\,2} + i\gamma_{ex}\omega$ and $\tilde{\omega}_{md}^{\,2} = \omega^2 - \omega_{md}^{\,2} + i\gamma_{md}\omega$ are the harmonic oscillator terms for the exciton and MD resonances, respectively, with ω_{ex}, ω_{md} and γ_{ex}, γ_{md} being the corresponding resonance frequencies and dissipation rates (full width at half-maximum). We also add an additional Lorentzian centered at ED resonance. After fitting the curve shown in Figure 1c, we obtain that the coupling constant $g \approx 58$ meV, whereas the dissipation rates equal $\gamma_{ex} \approx 33$ meV and $\gamma_{md} \approx 84$ meV.

It is known that in order to achieve strong coupling, the system should satisfy the criterion $\hbar\Omega > (\hbar\gamma_{ex} + \hbar\gamma_{md})/2$, where $\hbar\Omega$ is the Rabi splitting energy.[20,23] The coupling strength and Rabi splitting energy are related to each other via $g = \hbar\Omega/2$. In air, the total loss $\hbar\gamma_{ex} + \hbar\gamma_{md}$ is 117 meV, whereas the Rabi splitting energy $\hbar\Omega$ equals 116 meV, which satisfies the criterion $\hbar\Omega > (\hbar\gamma_{ex} + \hbar\gamma_{md})/2$. Thus, we come to the conclusion that in this case, the structure becomes strongly coupled. This conclusion is also supported by the Fano resonance lineshape analysis, which provides largely perturbed extracted resonant frequencies because of the interaction, a typical fingerprint of the strong coupling regime (for details, see the Supporting Information). Figure 1d demonstrates the dependency of the scattering cross section on the wavelength and coupling strength g of the Si NP-WS_2 core−shell system in air. The dashed line shows the value of the coupling strength in air. The other parameters of the system correspond to those obtained from our CMT fitting of the scattering spectrum (see Figure 1c). The figure shows that for the extracted coupling constant $g \approx 58$ meV, the spectrum became visibly split.

To further enhance the coupling strength, we propose to place the Si-WS_2 system in an environment (solvent) with a high static dielectric constant and utilize the dielectric screening effect[46,47] to increase the exciton dipole moment of 1L-WS_2. The coupling strength is proportional to the product of the exciton dipole moment d, number of excitons N, and the tangential component of the electric field near the sphere ($g \approx d \cdot N \cdot E_t$).[49−52] However, an exciton in 1L-WS_2 couples with the MD resonance in Si NPs at high frequencies (visible range), while the screening effect manifests at lower frequencies (depending on the exciton binding energy). Thus, the ideal background material for optimal coupling enhancement should possess a dielectric constant that is small at high frequencies and large at low frequencies. We find that water ideally fits this requirement because it has $\varepsilon_w \approx 1.77$ in the visible range and $\varepsilon_w \approx 78$ in the static limit. Moreover, in contrast to solids, water due to its liquid state interacts with 1L-WS_2 directly, avoiding air gaps.

Strictly speaking, according to the self-consistent many-body theory,[53−55] the effective potential of the electron−hole interaction should be taken at the frequency corresponding to the exciton binding energy. In conventional bulk semiconductors such as GaAs, the dielectric constant of the material is rather large (~13), which gives a small binding energy (~5 meV), and one could approximately use the static dielectric constant to describe the screening effect. However, 2D semiconductors (such as 1L-WS_2) in vacuum are essentially unscreened, thus possessing high binding energies up to ~800 meV. Even for 1L-WS_2 on a SiO_2 substrate it is ~400 meV, lying in the IR range. Nevertheless, some experiments on the dielectric screening of excitons in TMDC atomically thin monolayers[46,47] demonstrate good agreement with theoretical estimations based on static screening constants.

We estimate the enhancement of the exciton dipole moment in a 1L-WS_2 shell of the Si-WS_2 core−shell system embedded in water, using the static screening approximation. The Coulomb potential of the electron−hole interaction in TMDCs falls off at a distance of ≈2 nm (see the Supporting Information in ref 46), so we can treat the 150 nm Si NP as a flat substrate and consider the screening in 1L-WS_2 sandwiched between semi-infinite silicon (with static dielectric constant $\varepsilon_s = 11.7$) and water (with $\varepsilon_w = 78$ at $T = 300$ K). In this case, the exciton dipole moment is proportional to the effective dielectric constant $d_w \approx (\varepsilon_s + \varepsilon_w)/2$, while for the system in air it will be $d_a \approx (\varepsilon_s + 1)/2$. Notice that the field lines of an exciton in 2D semiconductors pass mainly through the environment, and

DOI: 10.1021/acsami.7b17112
ACS Appl. Mater. Interfaces XXXX, XXX, XXX−XXX

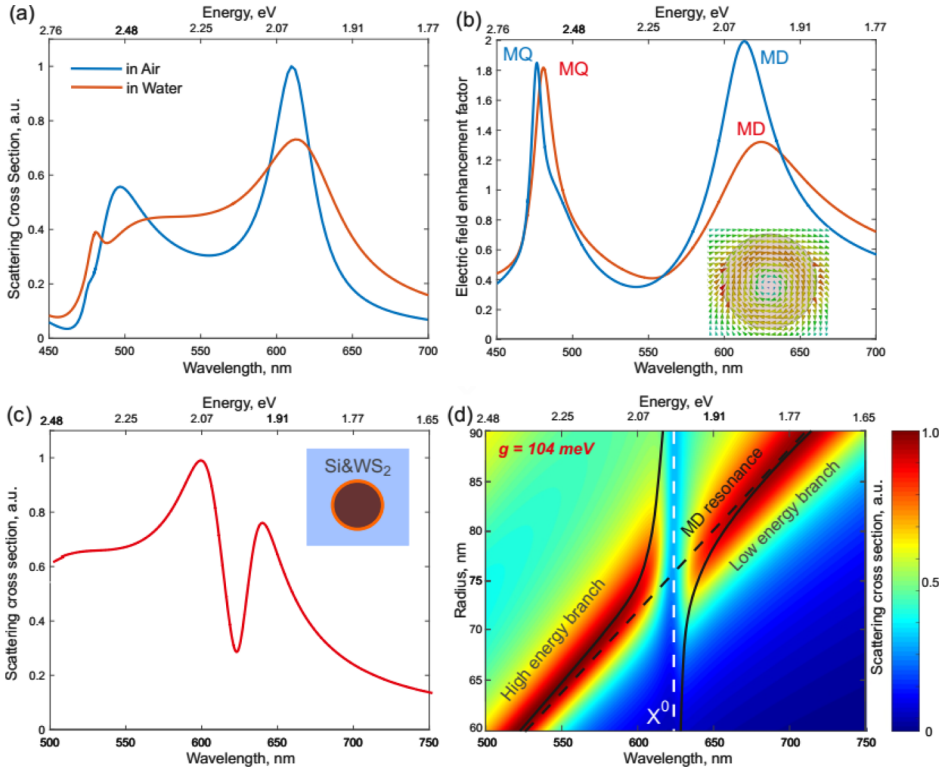

Figure 2. (a) Scattering cross sections of a spherical Si NP with radius R = 75 nm in air and in water environments. (b) Enhancement factor of the tangential electric field (E_t) near the Si sphere in air and in water environments. The inset shows the electric field at the MD resonance. (c) Scattering cross section of the Si-WS_2 core−shell system in water. (d) Scattering cross section of the Si-WS_2 core−shell system in water as a function on wavelength and Si NP radius.

thus, the screening is almost independent of the dielectric constant of the semiconductor, and it is completely determined by the surrounding media. Thus, assuming that the number of excitons does not change, the required enhancement of the dipole moment of a single exciton can be estimated by $(d_w/d_a)_{th} \approx (\varepsilon_s + \varepsilon_w)/(\varepsilon_s + 1) \approx 7$. However, due to the nonhydrogenic exciton behavior in TMDC[54] the exciton binding energy in them has an unusual scaling with the effective dielectric constant of the environment $E_b \sim 1/\varepsilon_{eff}$ at $\varepsilon_{eff} \gg 1$ [Komsa][48] insted of typical dependence $1/\varepsilon_{eff}^2$. Thus from $E_b \sim 1/d^2$ one can suppose that the dipole moment at $\varepsilon_{eff} \gg 1$ should be scaled as $d \sim \sqrt{\varepsilon_{eff}}$ giving the dipole moment enhancement $(d_w/d_a)_{th} \approx \sqrt{7} \approx 2.7$, which is in a good agreement with the experimentally obtained value (see the discussions of Figure 3d).

For the estimation of MD shifting, we calculate the scattering cross section of the spherical Si NP embedded in water using the Mie theory and compare it with the previous result in air, as shown in Figure 2a. For multipole decomposition, see the Supporting Information. We also calculate the enhancement factor of the *tangential electric field* (E_t) at the Si NP surface in air (blue curve) and in water (red curve). Figure 2b highlights that at the MD resonance, the value of E_t decreases by ∼1.5 times. We note that as the ED mode does not support a tangential electric field near the Si NP, it does not appear in the electric field spectra (see Figure 2b). The high-frequency peak corresponds to the MQ resonance, and it is barely affected by the environment, as it is more confined within the particle. For the calculation of the tangential electric field with the SiO_2 substrate, see the Supporting Information.

Thus, knowing the enhancement of the dipole moment of the exciton subsystem and the weakening of the tangential electric field of the MD mode, we can estimate the change of coupling constant $g_w/g_a \approx 2.7/1.5 \approx 1.8$ (for the same number of excitons). Then, by obtaining the frequency of the MD in water from Figure 2a and using CMT with $g = 58 \times 1.8 \approx 104$, we plot the scattering cross section of the Si NP-WS_2 core−shell system embedded in water (see Figure 2c). In this case, the Rabi splitting becomes much more obvious. The coupling constant in this system $g \approx 104$ meV (and Rabi splitting energy 208 meV), whereas the dissipation rates equal $\gamma_{ex} \approx 33$ meV and $\gamma_{md} \approx 173$ meV. Thus, we can conclude that for a Si NP-WS_2 core−shell system in water, the coupling became even stronger. Figure 2d shows the scattering cross section of the Si NP-WS_2 core−shell system in water as a function of wavelength and Si NP radius. These results confirm the expected anticrossing behavior of scattering at the intersection of excitonic (X^0) and MD resonances with high-energy and low-energy branches.

In order to experimentally demonstrate tunable resonance coupling for the single Si NP-1L-WS_2 heterostructures, we have realized experimentally the geometry of optically resonant spherical Si NPs arranged on 1L-WS_2 schematically shown in Figure 3a. We prepared 1L-WS_2 by CVD and then transferred it onto a glass substrate via the poly(methyl methacrylate) (PMMA)-based transfer method (for details of 1L-WS_2 preparation and transfer, see Methods and Supporting Information). Figure 3b shows an optical image of the 1L-WS_2 flake with deposed Si NPs. The monolayer nature of the WS_2 flake is confirmed by the strong PL signal (Figure 3d), which is typical for direct band gap semiconductors.[58] The PL

DOI: 10.1021/acsami.7b17112
ACS Appl. Mater. Interfaces XXXX, XXX, XXX−XXX

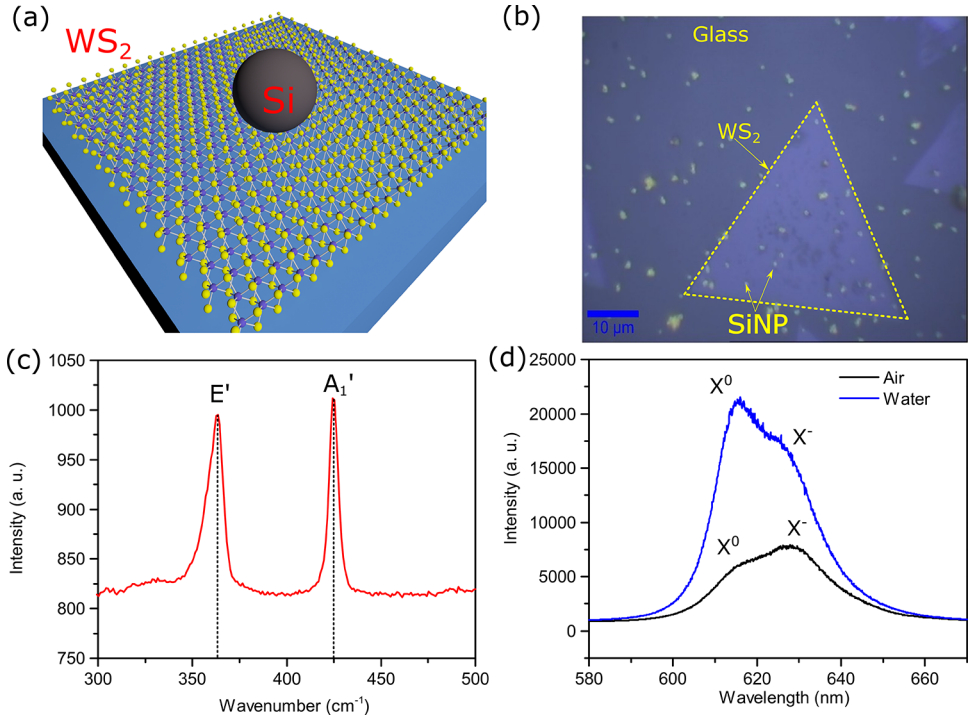

Figure 3. (a) Schematic view of a sample comprising a single Si NP on 1L-WS_2. (b) Optical image of 1L-WS_2 with deposed Si NPs. The scale bar is 10 μm. Raman (c) and PL (d) spectra of 1L-WS_2 on glass in air (the excitation wavelength is 488 nm).

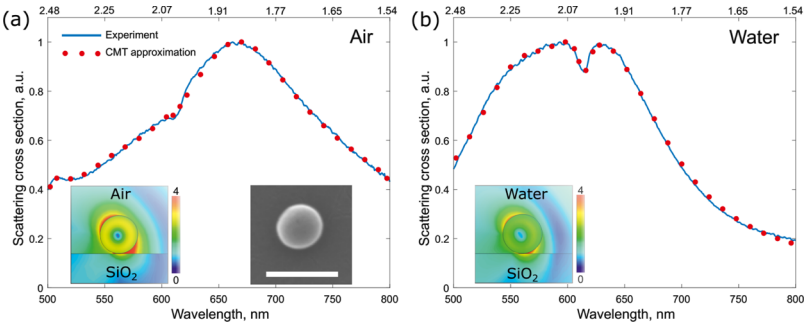

Figure 4. Experimentally measured (blue curve) and fitted by CMT (red dots) scattering spectra for single Si NP-1L-WS_2 heterostructures in air (a) and water (b). Left insets show the distribution profiles of absolute values of electric field at the wavelength of excitonic resonance (620 nm), which is close to the magnetic resonance of a-Si NPs. The right inset in (a) shows the SEM image of Si NPs on the WS_2 flake. The scale bar is 500 nm. The values of Rabi splitting energy obtained from fitting of the experimental data demonstrate a significant enhancement from 49.6 to 86.6 meV when replacing air by water.

spectrum of 1L-WS_2 on the glass substrate in air under ambient conditions shows a resonance at 620 nm (1.99 eV), corresponding to the X^0 exciton, which matches the reported emission of CVD-grown 1L-WS_2. Moreover, the spectrum has a resonance at the negatively charged X^- exciton (i.e., trion), which originates from a slight electrical doping of the glass substrate. Atomic force microscopy was also used to confirm the thickness of monolayered WS_2 (see the Supporting Information). The crystalline structure of 1L-WS_2 is also confirmed by Raman scattering (see Figure 3c). The Raman spectrum exhibits two peaks centered at 362 and 424 cm^{-1}, which correspond to the out-of-plane E′ mode and the in-plane A_1' mode of 1L-WS_2, respectively.[57,58]

The PL spectra shown in Figure 3d reveal a 7.5 times enhancement in the PL intensity of the bare 1L-WS_2 in water (see the Supporting Information for spectra fitting information). This allows us to estimate the change of dipole moment of a single exciton. To this end, we consider that the PL intensity I is proportional to the squared total dipole D moment of all excitons in the system $I \approx D^2 \approx (d \cdot N)^2$. The number of excited excitons N is proportional to the tangential electric field intensity on the TMDC surface, which is slightly changed in water because of Fresnel reflection, and this effect can be neglected. Thus, we estimate $(d_w/d_a)_{exp} \approx 2.7$, which is in a good agreement with the theoretical estimation obtained above using the static screening approximation.

Hydrogenated amorphous silicon (a-Si:H) NPs were synthesized in supercritical *n*-hexane (for details of a-Si:H NP preparation, see Methods and Supporting Information).[59] The right inset in Figure 4a shows the SEM image of Si NP arranged on the WS_2 flake. Figure 4 shows the experimentally measured (blue line) and simulated by CMT (red dots) scattering spectra for single Si NP-1L-WS_2 heterostructures in air (a) and water (b).[60] In the case of air, we observe a Fano-like scattering feature at the wavelength of the X^0-exciton resonance. The fitting by CMT gives the Rabi splitting energy of 49.6 meV in

DOI: 10.1021/acsami.7b17112
ACS Appl. Mater. Interfaces XXXX, XXX, XXX−XXX

this case. On the basis of the above discussion, we can expect a significant enhancement of the Rabi splitting energy when the system is placed in water. Indeed, in this second scenario, we achieve 86.6 meV. We emphasize that this experimentally measured value is much less than that expected for the core−shell geometry because of the significantly smaller number of excitons that take place in the resonance interaction. The obtained results correspond to the Fano resonance; for the detailed analysis and fitting the spectra by Fano lineshape, see the Supporting Information. Considering that the Si NP has only one point of contact with the TMDC surface, we may estimate the number of excited excitons to be only a few.

Finally, the experimentally measured increase of the coupling constant and Rabi splitting energy by ∼2 times is in good agreement with the increase of the PL spectra for water by a factor of 7.5 and the reduction of local electric field within a-Si NP and WS_2 flake by ∼1.3 times (see left insets in Figure 4). These distribution profiles show absolute values of the electric field at the wavelength of excitonic resonance (615 nm), which is close to the magnetic resonance of a-Si NP in air and water. The permittivity of amorphous silicon has been used for numerical calculations of the electric field distributions.

CONCLUSIONS

In conclusion, we have addressed the issue of resonance coupling in single Si NP−monolayer TMDC (WS_2) structures. We have theoretically predicted a strong coupling regime with a Rabi splitting energy exceeding 110 meV for a Si NP covered by 1L-WS_2 at the magnetic optical Mie resonance because of the symmetry of the mode. Further, we have achieved a large enhancement in the Rabi splitting energy up to 208 meV by changing the surrounding dielectric material from air to water. This prediction is based on the experimental estimation of the TMDC dipole moment change obtained from the measured PL spectra of the TMDC in different solvents. The ability of such a system to realize tunable resonance coupling has been experimentally verified using optically resonant spherical Si NPs placed on 1L-WS_2. The Rabi splitting energy obtained in this case increases from 49.6 up to 86.6 meV when replacing air by water as the background material. Our findings pave the way to a novel class of low-loss nanophotonic, optoelectronic, and quantum optical devices based on dielectric resonant NPs coupled with 2D excitonic materials.

Note added. Recently, we became aware of related works devoted to resonant photon−exciton coupling in a system composed of 1L-WS_2 and Si nanosphere in ref 61 and directional control over the emission from 1L-MoS_2 coupled to the Si nanowire in ref 62.

METHODS

1L-WS_2 Preparation. The atmospheric pressure CVD (APCVD) method was used to prepare 1L-WS_2 on SiO_2/Si wafers. A tube furnace with argon as the carrier gas (the flow rate is 150 sccm, during the synthesis) was employed. Two freshly cleaned SiO_2/Si wafers with ∼10 mg WO_3 powders sandwiched by them were placed in a 2 cm diameter quartz tube. Then, WO_3 powders were heated up to 700 °C and held for 15 min in the tube furnace, and simultaneously sulfur powders were separately heated up to 250 °C with a heating belt. Following the APCVD fabrication, the as-grown 1L-WS_2 was transferred onto a glass substrate. The transfer process began by spin-coating a layer of PMMA on as-grown 1L-WS_2 on the SiO_2/Si wafer. Then, the SiO_2/Si wafer was etched away by 1 M sodium hydroxide (NaOH) aqueous solution. After being rinsed with deionized water several times, the detached PMMA + WS_2 film was fished onto a precleaned glass substrate. Finally, the PMMA layer was removed by immersing the whole specimen into acetone. For more details, see the Supporting Information.

Synthesis of Si NPs. a-Si:H NPs were synthesized in supercritical *n*-hexane, as described previously.[63,64] A 10 mL titanium batch reactor purchased from High Pressure Equipment Company (HiP Co.) was brought in a nitrogen-filled glovebox. Trisilane (21 μL) and a certain amount of *n*-hexane were added in the reactor. In all reactions, the pressure was kept at 34.5 MPa (5000 psi). After loading the reagents, the reactor was first sealed using a wrench inside the glovebox. The reactor was then inserted into a heating block and heated to the target temperature for 10 min to allow complete decomposition of trisilane. After the reaction, the reactor was cooled to room temperature by an ice bath. The reactor was then opened, and the colloidal a-Si:H NPs were extracted from the reactor. The NPs were washed using chloroform by centrifuging at 8000 rpm for 5 min. The precipitate was collected and dispersed in chloroform before use. For more details, see the Supporting Information.

Optical Measurements. Si NPs were drop-casted on the bare glass substrate or the top of 1L-WS_2. The scattering spectra of single Si NPs on the bare glass substrate or 1L-WS_2 were measured by an inverted microscope (Ti-E, Nikon) with a spectrograph (Andor), an electron-multiplying charge-coupled device (Andor), and a halogen white light source (12V, 100 W), as schematically shown in Figure S3 (see the Supporting Information).[26,65,66] To measure the scattering spectra in the solvent with a big dielectric constant, water was sandwiched between the sample and a cover glass. The Witec micro-Raman spectrometer was also used to measure the PL spectra of 1L-WS_2 in different surrounding media. The power of the 488 nm laser we used to measure PL spectra is 1 mW.

ASSOCIATED CONTENT

Supporting Information

The Supporting Information is available free of charge on the ACS Publications website at DOI: 10.1021/acsami.7b17112.

Coupled mode theory, multipole decomposition, electric field enhancement for the Si NP on a SiO_2 substrate, fitting of spectra with Fano resonance, 1L-WS_2 preparation, and synthesis of Si NPs (PDF)

AUTHOR INFORMATION

Corresponding Authors

*E-mail: akrasnok@utexas.edu (A.K.).
*E-mail: zheng@austin.utexas.edu (Y.Z.).
*E-mail: alu@mail.utexas.edu (A.A.).

ORCID

Mingsong Wang: 0000-0001-9071-5517
Tianyi Zhang: 0000-0002-8998-3837
Brian Korgel: 0000-0001-6242-7526
Yuebing Zheng: 0000-0002-9168-9477
Andrea Alú: 0000-0002-4297-5274

Author Contributions

S.L., M.W., and A.K. contributed equally. S.L., A.K., M.W., Y.Z., and O.K. conceived the study and designed the experiments. S.L., A.K., and O.K. conducted the theoretical calculations. Y.Z., A.A., and M.W. participated in analysis of the theoretical and experimental data. T.J. and B.K. synthesized the silicon nanospheres. T.Z., H.L., and M.T. synthesized the WS_2 monolayers, conducted materials characterization and optimized the transferred process. O.K., A.K., A.A., and M.W. co-wrote the manuscript, with contributions from all authors. All authors have given approval to the final version of the manuscript.

DOI: 10.1021/acsami.7b17112
ACS Appl. Mater. Interfaces XXXX, XXX, XXX−XXX

Notes

The authors declare no competing financial interest.

■ ACKNOWLEDGMENTS

Y.Z. acknowledges the financial support of the Office of Naval Research Young Investigator Program (N00014-17-1-2424) and the National Science Foundation (NSF) Grant 1704634. M.T., T.Z., and H.L. thank NSF for the support through the EFRI 2-DARE Grant 1542707. M.W. acknowledges the financial support of GS University Graduate Continuing Fellowship. O.K. acknowledges the financial support of the Russian Science Foundation Grant No. 17-12-01393. A.K. and A.A. acknowledge the support from the Air Force Office of Scientific Research with MURI grant no. FA9550-17-1-0002 and the Welch Foundation with grant no. F-1802.

■ REFERENCES

(1) Wang, Y.; Knoll, W.; Dostalek, J. Bacterial Pathogen Surface Plasmon Resonance Biosensor Advanced by Long Range Surface Plasmons and Magnetic Nanoparticle Assays. *Anal. Chem.* **2012**, *84*, 8345−8350.

(2) Butler, S. Z.; Hollen, S. M.; Cao, L.; Cui, Y.; Gupta, J. A.; Gutiérrez, H. R.; Heinz, T. F.; Hong, S. S.; Huang, J.; Ismach, A. F.; Johnston-Halperin, E.; Kuno, M.; Plashnitsa, V. V.; Robinson, R. D.; Ruoff, R. S.; Salahuddin, S.; Shan, J.; Shi, L.; Spencer, M. G.; Terrones, M.; Windl, W.; Goldberger, J. E. Progress, Challenges, and Opportunities in Two-Dimensional Materials beyond Graphene. *ACS Nano* **2013**, *7*, 2898−2926.

(3) Xia, F.; Wang, H.; Xiao, D.; Dubey, M.; Ramasubramaniam, A. Two-Dimensional Material Nanophotonics. *Nat. Photonics* **2014**, *8*, 899−907.

(4) Mak, K. F.; Shan, J. Photonics and Optoelectronics of 2D Semiconductor Transition Metal Dichalcogenides. *Nat. Photonics* **2016**, *10*, 216−226.

(5) Bhimanapati, G. R.; Lin, Z.; Meunier, V.; Jung, Y.; Cha, J.; Das, S.; Xiao, D.; Son, Y.; Strano, M. S.; Cooper, V. R.; Liang, L.; Louie, S. G.; Ringe, E.; Zhou, W.; Kim, S. S.; Naik, R. R.; Sumpter, B. G.; Terrones, H.; Xia, F.; Wang, Y.; Zhu, J.; Akinwande, D.; Alem, N.; Schuller, J. A.; Schaak, R. E.; Terrones, M.; Robinson, J. A. Recent Advances in Two-Dimensional Materials beyond Graphene. *ACS Nano* **2015**, *9*, 11509−11539.

(6) Das, S.; Robinson, J. A.; Dubey, M.; Terrones, H.; Terrones, M. Beyond Graphene: Progress in Novel Two-Dimensional Materials and van Der Waals Solids. *Annu. Rev. Mater. Res.* **2015**, *45*, 1−27.

(7) Zhao, W.; Ghorannevis, Z.; Chu, L.; Toh, M.; Kloc, C.; Tan, P.-H.; Eda, G. Evolution of Electronic Structure in Atomically Thin Sheets of WS2 and WSe2. *ACS Nano* **2013**, *7*, 791−797.

(8) Lopez-Sanchez, O.; Lembke, D.; Kayci, M.; Radenovic, A.; Kis, A. Ultrasensitive Photodetectors Based on Monolayer MoS2. *Nat. Nanotechnol.* **2013**, *8*, 497−501.

(9) Britnell, L.; Ribeiro, R. M.; Eckmann, A.; Jalil, R.; Belle, B. D.; Mishchenko, A.; Kim, Y.-J.; Gorbachev, R. V.; Georgiou, T.; Morozov, S. V.; Grigorenko, A. N.; Geim, A. K.; Casiraghi, C.; Neto, A. H. C.; Novoselov, K. S. Strong Light-Matter Interactions in Heterostructures of Atomically Thin Films. *Science* **2013**, *340*, 1311−1314.

(10) Perea-Lõpez, N.; Elías, A. L.; Berkdemir, A.; Castro-Beltran, A.; Gutiérrez, H. R.; Feng, S.; Lv, R.; Hayashi, T.; Lõpez-Urías, F.; Ghosh, S.; Muchharla, B.; Talapatra, S.; Terrones, H.; Terrones, M. Photosensor Device Based on Few-Layered WS_2 Films. *Adv. Funct. Mater.* **2013**, *23*, 5511−5517.

(11) Koppens, F. H. L.; Mueller, T.; Avouris, P.; Ferrari, A. C.; Vitiello, M. S.; Polini, M. Photodetectors Based on Graphene, Other Two-Dimensional Materials and Hybrid Systems. *Nat. Nanotechnol.* **2014**, *9*, 780−793.

(12) Yin, Z.; Li, H.; Li, H.; Jiang, L.; Shi, Y.; Sun, Y.; Lu, G.; Zhang, Q.; Chen, X.; Zhang, H. Single-Layer MoS 2 Phototransistors. *ACS Nano* **2012**, *6*, 74−80.

(13) Sun, Z.; Martinez, A.; Wang, F. Optical Modulators with 2D Layered Materials. *Nat. Photonics* **2016**, *10*, 227−238.

(14) Lopez-Sanchez, O.; Llado, E. A.; Koman, V.; Morral, A. F. i.; Radenovic, A.; Kis, A. Light Generation and Harvesting in a van Der Waals Heterostructure. *ACS Nano* **2014**, *8*, 3042−3048.

(15) Withers, F.; Del Pozo-Zamudio, O.; Mishchenko, A.; Rooney, A. P.; Gholinia, A.; Watanabe, K.; Taniguchi, T.; Haigh, S. J.; Geim, A. K.; Tartakovskii, A. I.; Novoselov, K. S. Light-Emitting Diodes by Band-Structure Engineering in van Der Waals Heterostructures. *Nat. Mater.* **2015**, *14*, 301−306.

(16) Liu, C.-H.; Clark, G.; Fryett, T.; Wu, S.; Zheng, J.; Hatami, F.; Xu, X.; Majumdar, A. Nanocavity Integrated van Der Waals Heterostructure Light-Emitting Tunneling Diode. *Nano Lett.* **2017**, *17*, 200−205.

(17) Ye, Y.; Wong, Z. J.; Lu, X.; Ni, X.; Zhu, H.; Chen, X.; Wang, Y.; Zhang, X. Monolayer Excitonic Laser. *Nat. Photonics* **2015**, *9*, 733−737.

(18) Wu, S.; Buckley, S.; Schaibley, J. R.; Feng, L.; Yan, J.; Mandrus, D. G.; Hatami, F.; Yao, W.; Vučković, J.; Majumdar, A.; Xu, X. Monolayer Semiconductor Nanocavity Lasers with Ultralow Thresholds. *Nature* **2015**, *520*, 69−72.

(19) Krasnok, A.; Lepeshov, S.; Alú, A. Nanophotonics with 2D Transition Metal Dichalcogenides *Optics Express* **2018**, In press.

(20) Wen, J.; Wang, H.; Wang, W.; Deng, Z.; Zhuang, C.; Zhang, Y.; Liu, F.; She, J.; Chen, J.; Chen, H.; Deng, S.; Xu, N. Room-Temperature Strong Light−Matter Interaction with Active Control in Single Plasmonic Nanorod Coupled with Two-Dimensional Atomic Crystals. *Nano Lett.* **2017**, *17*, 4689−4697.

(21) Wang, S.; Li, S.; Chervy, T.; Shalabney, A.; Azzini, S.; Orgiu, E.; Hutchison, J. A.; Genet, C.; Samorì, P.; Ebbesen, T. W. Coherent Coupling of WS_2 Monolayers with Metallic Photonic Nanostructures at Room Temperature. *Nano Lett.* **2016**, *16*, 4368−4374.

(22) Zheng, D.; Zhang, S.; Deng, Q.; Kang, M.; Nordlander, P.; Xu, H. Manipulating Coherent Plasmon-Exciton Interaction in a Single Silver Nanorod on Monolayer WSe2. *Nano Lett.* **2017**, *17*, 3809−3814.

(23) Baranov, D. G.; Wersäll, M.; Cuadra, J.; Antosiewicz, T. J.; Shegai, T. Novel Nanostructures and Materials for Strong Light−Matter Interactions. *ACS Photonics* **2018**, *5*, 24−42.

(24) Kleemann, M.-E.; Chikkaraddy, R.; Alexeev, E. M.; Kos, D.; Carnegie, C.; Deacon, W.; de Pury, A. C.; Große, C.; de Nijs, B.; Mertens, J.; Tartakovskii, A. I.; Baumberg, J. J. Strong-Coupling of WSe2 in Ultra-Compact Plasmonic Nanocavities at Room Temperature. *Nat. Commun.* **2017**, *8*, 1296.

(25) Abid, I.; Chen, W.; Yuan, J.; Bohloul, A.; Najmaei, S.; Avendano, C.; Péchou, R.; Mlayah, A.; Lou, J. Temperature-Dependent Plasmon-Exciton Interactions in Hybrid Au/MoSe2 Nanostructures. *ACS Photonics* **2017**, *4*, 1653−1660.

(26) Wang, M.; Li, W.; Scarabelli, L.; Rajeeva, B. B.; Terrones, M.; Liz-Marzán, L. M.; Akinwande, D.; Zheng, Y. Plasmon−trion and Plasmon−exciton Resonance Energy Transfer from a Single Plasmonic Nanoparticle to Monolayer MoS2. *Nanoscale* **2017**, *9*, 13947−13955.

(27) Naik, G. V.; Shalaev, V. M.; Boltasseva, A. Alternative Plasmonic Materials: Beyond Gold and Silver. *Adv. Mater.* **2013**, *25*, 3264−3294.

(28) Khurgin, J. B. How to Deal with the Loss in Plasmonics and Metamaterials. *Nat. Nanotechnol.* **2015**, *10*, 2−6.

(29) Kuznetsov, A. I.; Miroshnichenko, A. E.; Brongersma, M. L.; Kivshar, Y. S.; Luk'yanchuk, B. Optically Resonant Dielectric Nanostructures. *Science* **2016**, *354*, aag2472.

(30) Baranov, D. G.; Zuev, D. A.; Lepeshov, S. I.; Kotov, O. V.; Krasnok, A. E.; Evlyukhin, A. B.; Chichkov, B. N. All-Dielectric Nanophotonics: The Quest for Better Materials and Fabrication Techniques. *Optica* **2017**, *4*, 814.

(31) Evlyukhin, A. B.; Novikov, S. M.; Zywietz, U.; Eriksen, R. L.; Reinhardt, C.; Bozhevolnyi, S. I.; Chichkov, B. N. Demonstration of Magnetic Dipole Resonances of Dielectric Nanospheres in the Visible Region. *Nano Lett.* **2012**, *12*, 3749−3755.

DOI: 10.1021/acsami.7b17112
ACS Appl. Mater. Interfaces XXXX, XXX, XXX−XXX

(32) Zywietz, U.; Schmidt, M. K.; Evlyukhin, A. B.; Reinhardt, C.; Aizpurua, J.; Chichkov, B. N. Electromagnetic Resonances of Silicon Nanoparticle Dimers in the Visible. *ACS Photonics* **2015**, *2*, 913−920.
(33) Jahani, S.; Jacob, Z. All-Dielectric Metamaterials. *Nat. Nanotechnol.* **2016**, *11*, 23−36.
(34) Krasnok, A. E.; Miroshnichenko, A. E.; Belov, P. A.; Kivshar, Y. S. All-Dielectric Optical Nanoantennas. *Opt. Express* **2012**, *20*, 20599.
(35) Staude, I.; Khardikov, V. V.; Fofang, N. T.; Liu, S.; Decker, M.; Neshev, D. N.; Luk, T. S.; Brener, I.; Kivshar, Y. S. Shaping Photoluminescence Spectra with Magnetoelectric Resonances in All-Dielectric Nanoparticles. *ACS Photonics* **2015**, *2*, 172−177.
(36) Li, Y.; Cain, J. D.; Hanson, E. D.; Murthy, A. A.; Hao, S.; Shi, F.; Li, Q.; Wolverton, C.; Chen, X.; Dravid, V. P. Au@MoS2 Core-Shell Heterostructures with Strong Light-Matter Interactions. *Nano Lett.* **2016**, *16*, 7696−7702.
(37) Mi, Y.; Zhang, Z.; Zhao, L.; Zhang, S.; Chen, J.; Ji, Q.; Shi, J.; Zhou, X.; Wang, R.; Shi, J.; Du, W.; Wu, Z.; Qiu, X.; Zhang, Q.; Zhang, Y.; Liu, X. Tuning Excitonic Properties of Monolayer MoS_2 with Microsphere Cavity by High-Throughput Chemical Vapor Deposition Method. *Small* **2017**, *13*, 1701694.
(38) Bohren, C. F.; Huffman, D. R. *Absorption and Scattering of Light by Small Particles*; Bohren, C. F., Huffman, D. R., Eds.; Wiley-VCH Verlag GmbH: Weinheim: Germany, 1998.
(39) Li, Y.; Chernikov, A.; Zhang, X.; Rigosi, A.; Hill, H. M.; van der Zande, A. M.; Chenet, D. A.; Shih, E.-M.; Hone, J.; Heinz, T. F. Measurement of the Optical Dielectric Function of Monolayer Transition-Metal Dichalcogenides: MoS2, MoSe2, WS2, and WSe2. *Phys. Rev. B: Condens. Matter Mater. Phys.* **2014**, *90*, 205422.
(40) Vuye, G.; Fisson, S.; Nguyen Van, V.; Wang, Y.; Rivory, J.; Abelès, F. Temperature Dependence of the Dielectric Function of Silicon Using in Situ Spectroscopic Ellipsometry. *Thin Solid Films* **1993**, *233*, 166−170.
(41) Savelev, R. S.; Sergaeva, O. N.; Baranov, D. G.; Krasnok, A. E.; Alù, A. Dynamically Reconfigurable Metal-Semiconductor Yagi-Uda Nanoantenna. *Phys. Rev. B* **2017**, *95*, 235409.
(42) Alù, A.; Engheta, N. Polarizabilities and Effective Parameters for Collections of Spherical Nanoparticles Formed by Pairs of Concentric Double-Negative, Single-Negative, Andor Double-Positive Metamaterial Layers. *J. Appl. Phys.* **2005**, *97*, 094310.
(43) Aden, A. L.; Kerker, M. Scattering of Electromagnetic Waves from Two Concentric Spheres. *J. Appl. Phys.* **1951**, *22*, 1242−1246.
(44) Zengin, G.; Johansson, G.; Johansson, P.; Antosiewicz, T. J.; Käll, M.; Shegai, T. Approaching the Strong Coupling Limit in Single Plasmonic Nanorods Interacting with J-Aggregates. *Sci. Rep.* **2013**, *3*, 3074.
(45) Wu, X.; Gray, S. K.; Pelton, M. Quantum-Dot-Induced Transparency in a Nanoscale Plasmonic Resonator. *Opt. Express* **2010**, *18*, 23633.
(46) Lin, Y.; Ling, X.; Yu, L.; Huang, S.; Hsu, A. L.; Lee, Y.-H.; Kong, J.; Dresselhaus, M. S.; Palacios, T. Dielectric Screening of Excitons and Trions in Single-Layer MoS2. *Nano Lett.* **2014**, *14*, 5569−5576.
(47) Mao, N.; Chen, Y.; Liu, D.; Zhang, J.; Xie, L. Solvatochromic Effect on the Photoluminescence of MoS2 Monolayers. *Small* **2013**, *9*, 1312−1315.
(48) Kylanpaa, I.; Komsa, H.-P. Binding energies of exciton complexes in transition metal dichalcogenide monolayers and effect of dielectric environment. *Phys. Rev. B: Condens. Matter Mater. Phys.* **2015**, *92*, 205418.
(49) Marquier, F.; Sauvan, C.; Greffet, J.-J. Revisiting Quantum Optics with Surface Plasmons and Plasmonic Resonators. *ACS Photonics* **2017**, *4*, 2091−2101.
(50) Słowik, K.; Filter, R.; Straubel, J.; Lederer, F.; Rockstuhl, C. Strong Coupling of Optical Nanoantennas and Atomic Systems. *Phys. Rev. B: Condens. Matter Mater. Phys.* **2013**, *88*, 195414.
(51) Chikkaraddy, R.; de Nijs, B.; Benz, F.; Barrow, S. J.; Scherman, O. A.; Rosta, E.; Demetriadou, A.; Fox, P.; Hess, O.; Baumberg, J. J. Single-Molecule Strong Coupling at Room Temperature in Plasmonic Nanocavities. *Nature* **2016**, *535*, 127−130.
(52) Zhou, N.; Yuan, M.; Gao, Y.; Li, D.; Yang, D. Silver Nanoshell Plasmonically Controlled Emission of Semiconductor Quantum Dots in the Strong Coupling Regime. *ACS Nano* **2016**, *10*, 4154−4163.
(53) Mahan, G. D. *Many-Particle Physics*; Springer US: Boston, MA, 2000.
(54) Stier, A. V.; Wilson, N. P.; Clark, G.; Xu, X.; Crooker, S. A. Probing the Influence of Dielectric Environment on Excitons in Monolayer WSe2: Insight from High Magnetic Fields. *Nano Lett.* **2016**, *16*, 7054−7060.
(55) Wang, G.; Chernikov, A.; Glazov, M. M.; Heinz, T. F.; Marie, X.; Amand, T.; Urbaszek, B. Excitons in Atomically Thin Transition Metal Dichalcogenides. **2017**, arXiv:1707.05863.
(56) Zhang, Y.; Zhang, Y.; Ji, Q.; Ju, J.; Yuan, H.; Shi, J.; Gao, T.; Ma, D.; Liu, M.; Chen, Y.; Song, X.; Hwang, H. Y.; Cui, Y.; Liu, Z. Controlled Growth of High-Quality Monolayer WS_2 Layers on Sapphire and Imaging Its Grain Boundary. *ACS Nano* **2013**, *7*, 8963−8971.
(57) Del Corro, E.; Botello-Méndez, A.; Gillet, Y.; Elias, A. L.; Terrones, H.; Feng, S.; Fantini, C.; Rhodes, D.; Pradhan, N.; Balicas, L.; Gonze, X.; Charlier, J.-C.; Terrones, M.; Pimenta, M. A. Atypical Exciton-Phonon Interactions in WS_2 and WSe_2 Monolayers Revealed by Resonance Raman Spectroscopy. *Nano Lett.* **2016**, *16*, 2363−2368.
(58) Carvalho, B. R.; Wang, Y.; Mignuzzi, S.; Roy, D.; Terrones, M.; Fantini, C.; Crespi, V. H.; Malard, L. M.; Pimenta, M. A. Intervalley Scattering by Acoustic Phonons in Two-Dimensional MoS2 Revealed by Double-Resonance Raman Spectroscopy. *Nat. Commun.* **2017**, *8*, 14670.
(59) Shi, L.; Harris, J. T.; Fenollosa, R.; Rodriguez, I.; Lu, X.; Korgel, B. A.; Meseguer, F. Monodisperse Silicon Nanocavities and Photonic Crystals with Magnetic Response in the Optical Region. *Nat. Commun.* **2013**, *4*, 1904.
(60) Wang, M.; Krasnok, A.; Zhang, T.; Scarabelli, L.; Liu, H.; Wu, Z.; Liz-Marzan, L. M.; Terrones, M.; Alu, A.; Zheng, Y. Tunable Fano Resonance and Plasmon-Exciton Coupling in Single Au Nanotriangles on Monolayer WS 2 at Room Temperature. *Adv. Mater.* **2018**, in press.DOI: 10.1002/adma.201705779.
(61) Wang, H.; Wen, J.; Liu, P.; Yan, J.; Zhang, Y.; Liu, F.; She, J. Resonant Photon-Exciton Coupling in All-Semiconductor Heterostructures Composed of Silicon Nanosphere and Monolayer WS_2. **2017**, 1−29, arXiv:1710.11447.
(62) F. Cihan, A.; Curto, A. G.; Raza, S.; Kik, P. G.; Brongersma, M. L. Silicon Mie Resonators for Highly Directional Light Emission from Monolayer MoS2. **2017**, 1−31, arXiv:1709.04999.
(63) Pell, L. E.; Schricker, A. D.; Mikulec, F. V.; Korgel, B. A. Synthesis of Amorphous Silicon Colloids by Trisilane Thermolysis in High Temperature Supercritical Solvents. *Langmuir* **2004**, *20*, 6546−6548.
(64) Harris, J. T.; Hueso, J. L.; Korgel, B. A. Hydrogenated Amorphous Silicon (a-Si:H) Colloids. *Chem. Mater.* **2010**, *22*, 6378−6383.
(65) Wang, M.; Hartmann, G.; Wu, Z.; Scarabelli, L.; Rajeeva, B. B.; Jarrett, J. W.; Perillo, E. P.; Dunn, A. K.; Liz-Marzán, L. M.; Hwang, G. S.; Zheng, Y. Controlling Plasmon-Enhanced Fluorescence via Intersystem Crossing in Photoswitchable Molecules. *Small* **2017**, *13*, 1701763.
(66) Wang, M.; Rajeeva, B. B.; Scarabelli, L.; Perillo, E. P.; Dunn, A. K.; Liz-Marzán, L. M.; Zheng, Y. Molecular-Fluorescence Enhancement via Blue-Shifted Plasmon-Induced Resonance Energy Transfer. *J. Phys. Chem. C* **2016**, *120*, 14820−14827.

DOI: 10.1021/acsami.7b17112
ACS Appl. Mater. Interfaces XXXX, XXX, XXX−XXX